



Published in final edited form as:

Bioorg Med Chem. 2018 October 01; 26(18): 4984–4995. doi:10.1016/j.bmc.2018.08.020.

Development of matrix metalloproteinase-13 inhibitors – A structure-activity/structure-property relationship study

Rita Fuerst^{a,c}, Jun Yong Choi^{a,d}, Anna M. Knapinska^b, Lyndsay Smith^b, Michael D. Cameron^a, Claudia Ruiz^a, Gregg B. Fields^b, and William R. Roush^a

^aDepartment of Chemistry, Scripps Florida, Jupiter, Florida 33458, United States

^bDepartment of Chemistry & Biochemistry, Florida Atlantic University, Jupiter, Florida 33458, United States

^cInstitute of Organic Chemistry, Graz University of Technology, 8010 Graz, Austria

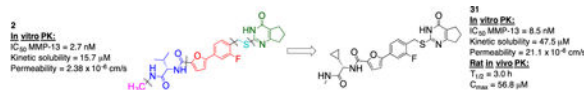
^dDepartment of Chemistry and Biochemistry, Queens College and the Graduate Center of the City University of New York, New York 11367, United States

Abstract

A structure-activity/structure-property relationship study based on the physicochemical as well as *in vitro* pharmacokinetic properties of a first generation matrix metalloproteinase (MMP)-13 inhibitor (**2**) was undertaken. After systematic variation of inhibitor **2**, compound **31** was identified which exhibited microsomal half-life higher than **20** min, kinetic solubility higher than 20 μM , and a permeability coefficient greater than 20×10^{-6} cm/s. Compound **31** also showed excellent *in vivo* PK properties after IV dosing ($C_{\text{max}} = 56.8 \mu\text{M}$, $T_{1/2}(\text{plasma}) = 3.0$ h, $\text{Cl} = 0.23$ mL/min/kg) and thus is a suitable candidate for *in vivo* efficacy studies in an OA animal model.

Graphical Abstract

To create your abstract, type over the instructions in the template box below. Fonts or abstract dimensions should not be changed or altered.



Keywords

Matrix metalloproteinase 13; Structure-property relationship; Structure-activity relationship; Microsomal stability; Solubility; Permeability; *In vitro* and *in vivo* pharmacokinetics

Supplementary Material

All procedures for the synthesis of the compounds presented in the manuscript as well as methods and experimental details can be found in the Supplementary data associated with this article at <https://>

Publisher's Disclaimer: This is a PDF file of an unedited manuscript that has been accepted for publication. As a service to our customers we are providing this early version of the manuscript. The manuscript will undergo copyediting, typesetting, and review of the resulting proof before it is published in its final citable form. Please note that during the production process errors may be discovered which could affect the content, and all legal disclaimers that apply to the journal pertain.

1. Introduction

Osteoarthritis (OA), the degeneration of cartilage, is the most common disabling condition in the Western world.¹ Several risk factors such as genetic predisposition, obesity, and joint malalignment are associated with OA while the pathogenesis of cartilage degeneration remains largely unexplained.² In principle, any synovial joint in the human body can be affected by OA, but commonly the larger, weight-bearing joints such as the hips, knees, and the lumbar region of the spine are mostly targeted. Clinically, pain and stiffness of affected joints with up to complete loss of mobility are the main symptoms of OA. So far, medical treatment options are rather limited and are mainly focused on relieving pain to maintain motoric and functional capabilities.³ Therefore, oral analgesics, especially paracetamol, ibuprofen, and celecoxib, which are all non-steroidal anti-inflammatory drugs (NSAID) and selective COX-2 inhibitors, are the first-choice drugs for the treatment of OA.⁴ These treatment options are ultimately ineffective because the biochemical mechanisms responsible for cartilage degeneration are not addressed. Therefore, there is an urgent need for the development of disease modifying agents to increase the quality of life for OA patients. Despite intensive academic and industrial research over the past years the problem still remains unsolved.⁵

Several zinc-dependent matrix metalloproteinases (MMPs) are known to play crucial roles in the turnover of extracellular matrix (ECM) and the associated destruction of articular cartilage in OA.⁶ In particular, the role of MMP-13, which is also known as human collagenase-3, has been extensively analyzed and the enzyme shown to be primarily responsible for the cleavage of type II collagen in OA.⁷

Multiple attempts at developing an MMP-13 inhibitor-based therapeutic have failed mostly due to dose limiting side effects collectively described as musculoskeletal syndrome (MSS).⁸ The exact cause of MSS is not known. It is believed that the zinc-chelating properties of the first generation MMP inhibitors evoked a lack of selectivity toward other metalloproteases and/or non-related proteins.⁸ As a consequence, compounds lacking zinc chelating groups have been screened to identify inhibitors that did not suffer from non-specific binding. Several selective, nonzinc chelating MMP-13 inhibitors have been reported and biologically evaluated.⁹ Although all of these compounds showed very impressive selectivity profiles toward MMP-13, none has yet completed clinical trials. Co-crystal structural analysis and molecular modeling studies indicate that most of the non-zinc chelating compounds modulated the activity of MMP-13 by binding within a “specificity pocket” (subsite S1') and its surrounding loop (S1' specificity loop or Ω -loop).^{9d, 10}

An initial high-throughput screening (HTS) effort at the Scripps Research Institute, as part of the Molecular Libraries Probe Production Centers Network (MLPCN) program, followed by a first round of medicinal chemistry efforts identified compound **1** (Figure 1A), a 2.4 μM inhibitor of MMP-13.¹¹ The X-ray co-crystal structure of MMP-13 in complex with **1** revealed that the inhibitor bound within the known S1' subsite.¹² The *p*-methylphenyl ring points toward the catalytic center and shows a π - π stacking interaction with one of the imidazole rings, which coordinates the MMP-13 active site zinc ion (Figure 1B). Furthermore, the cyclopentyl moiety of the pyrimidinone unit of **1** is oriented toward the S1'

specificity loop.^{9d} Using this cocrystal structure for design purposes, we recently reported a three-step approach for the development of highly potent and selective MMP-13 inhibitors.¹³ In steps one and two we applied comparative structural analyses followed by molecular design to obtain non-selective but highly potent Zn²⁺-chelating compounds. In the third step the chelating moiety was removed to increase selectivity. This approach resulted in the synthesis of a set of compounds, including **2**, which exhibit a 1000-fold improvement of inhibitory potency compared to **1**. Due to the assumption that off-target inhibition of zinc containing enzymes plays a pivotal role in MSS, **2** was screened against a panel of more than 25 proteases, including MMP-1, MMP-2, MMP-8, MMP-9, and MT1-MMP, which are able to cleave collagen¹⁴ and are the closest relatives of MMP-13 with sequence homologies higher than 60%. At a concentration of 5 μ M, inhibitor **2** did not inhibit any protease outside the MMP-family. Even within the MMP- family, **2** showed ca. 1000-fold selectivity versus the other MMPs screened (Figure 1A).¹³

Based on the physicochemical as well as *in vitro* pharmacokinetic (PK) properties of **2** we have performed and report herein a systematic variation of this inhibitor scaffold and investigated the influence of the structural modifications within a structure-activity relationship (SAR)/structure-property relationship (SPR) study. Our final goal was to obtain a set of compounds suitable for *in vivo* testing in an OA animal model.

2. Results and Discussion

The kinetic solubility, permeability through an artificial membrane (PAMPA assay)¹⁵, $\text{clogD}_{7.4}$ and clogP values, and *in vitro* stability in human, rat, and mouse liver microsomes for **2** were determined (Table 1). These data were used to focus a SAR/SPR study to design selective MMP-13 inhibitors with improved pharmacokinetic (PK) properties. The goal was to reach the following *in vitro* property benchmarks before evaluating compounds further in *in vivo* PK experiments: (A) at least 20 min *in vitro* half-life ($t_{1/2}$) in liver microsomes;¹⁶ (B) kinetic solubility higher than 15 μ M as well as permeability coefficients greater than 20×10^{-6} cm/s;¹⁶ and (C) clogP and $\text{clogD}_{7.4}$ values in the 0–3 and 1–4 range, respectively, values viewed as suitable for passive diffusion after oral dosing.¹⁷

The kinetic solubility of **2** (15.7 μ M) as well as the clogP and $\text{clogD}_{7.4}$ values (3.0 and 4.2) represented the lower and upper limits of the desired ranges, respectively. Compound **2** showed a moderate permeability value (2.38×10^{-6} cm/s) and a retention in the lipid bilayer of 47%. The *in vitro* half-life of **2** in human, mouse, and rat liver microsomes was 12, 20, and 9 min, respectively. (Sutent was used as a reference for all microsome stability studies, and its half-life was 75, 13, and 34 min in human, mouse, and rat microsomes, respectively¹⁸).

As compounds exhibiting low *in vitro* metabolic stabilities ($t_{1/2}$) tend to have high *in vivo* clearance rates and poor *in vivo* PK properties,¹⁹ increasing the metabolic stability of **2** by removing metabolically labile groups was the first focus of the present study. The monooxygenases of the P450 family in the liver and intestine are the most important enzymes for drug metabolism.²⁰ The binding sites of these enzymes are generally lipophilic and interact preferably with lipophilic molecules.²¹ To improve the metabolic stability of **2**

we wanted to reduce the overall lipophilicity (lower clogP and clogD_{7.4}) and remove or block labile groups and metabolically vulnerable sites at the same time.²¹ Therefore, the determination of *in vitro* half-life in human, mouse, and rat liver microsomes was used to assess the *in vivo* metabolic stability of new compounds. In principle, the reduction of clogP and clogD_{7.4} values by adding more polar atoms or groups would also help to increase the solubility of the inhibitor analogs.

Compound **2** was divided into five parts: (1) the terminal methylamine group (Figure 2, pink), (2) the amino acid part (Figure 2, blue), (3) the phenyl-furan group (Figure 2, red), (4) the carbon-sulfur linker (Figure 2, turquoise), and (5) the pyrimidinone scaffold (Figure 2, green). We designed and synthesized analogs of **2** by varying these five subunits in order to systematically study SAR and SPR.

All synthesized compounds were first analyzed for their inhibitory activity against MMP-1, MMP-2, MMP-8, MMP-9, MMP-13, and MT1-MMP catalyzed hydrolysis of the triple-helical collagen mimic substrate fTHP-15^{12, 22}, followed by the determination of the inhibition of type II collagen cleavage at an inhibitor concentration of 20 μM. Compounds exhibiting at least 5-fold selectivity for MMP-13 and >90% inhibition of collagen cleavage at 20 μM were investigated for their metabolic stability in human, mouse, and rat liver microsomes as a guideline to assess their *in vivo* hepatic stability.

Variation of the terminal methylamine unit.

According to the co-crystal structure of MMP13•(*S*)-**3** (Figure 1C), the terminal methylamine group of the inhibitor reaches into a substrate binding area of MMP-13 without direct interaction with the target structure. Thus, the terminal part of **2** is a desired location to install polar groups to improve solubility and microsomal stability. A series of compounds was prepared (Scheme 1 and Table 2). Briefly, the Suzuki reaction of bromofuran **4** and boronic acid **5** was followed by a benzylic bromination reaction. Substitution of the bromide with thiopyrimidone **6** gave methyl ester **7**, which was hydrolyzed under basic conditions. Subsequent amino acid coupling with different valine derivatives resulted in the synthesis of 15 analogs (Table 2).¹³

The IC₅₀ values for inhibition of MMP-13 catalyzed hydrolysis of fTHP-15^{12, 22}, the selectivity profile among the remaining collagenases (MMP-1, MMP-2, MMP-8, MMP-9, and MT1-MMP), and the *in vitro* microsomal stability in human, mouse, and rat liver microsomes of the synthesized compounds were evaluated (Table 2). All compounds exhibited IC₅₀ values for MMP-13 in the low nanomolar range and higher than 10-fold selectivities among the collagenases compared to MMP-13. Interestingly, substituting the methylamine group with polar residues and changing the stereochemistry in the amino acid component (as in the enantiomeric pairs **9/10** and **15/16** as well as the diastereomeric pairs **11/12** and **13/14**) did not influence the potency of these compounds toward MMP-13 but did impact the selectivity profile negatively compared to **2**. Compounds **21**, **22**, and **23** showed no inhibition of fTHP-15 hydrolysis by MMP-1, MMP-2, MMP-8, MMP-9, and MT1-MMP at 5 μM, which was the highest concentration tested. Furthermore, all compounds except **19** and **20** (IC₅₀ > 5 μM in the fTHP-15 assay) were able to inhibit collagen cleavage by >95%

at a concentration of 20 μM . Compounds **18** and **21** exhibited acceptable stability in mouse and rat liver microsomes ($t_{1/2}$ for **18** = 26 and 34 min in mouse and rat, respectively, while $t_{1/2}$ for **21** = 22 and 42 min in mouse and rat, respectively), but the stability in human microsomes was lower ($t_{1/2}$ = 13 and 14 min for **18** and **21**, respectively). Compounds **22** and **23** showed excellent selectivity within the MMP family and very desirable *in vitro* stabilities in rat and human microsomes (Table 2).

Variation of the amino acid unit of compound 2.

In the next step, we modified the amino acid component of **2** by coupling **24** with different amino acid derivatives (Scheme 2, Table 3). Hydrolysis by proteases or peptidases can contribute to drug degradation in the plasma as well as the gastrointestinal tract.²³ Avoiding amide bonds or shielding them with adjacent bulky groups are common structural modification strategies to lower the hydrolysis rate of a compound. Furthermore, if an amino acid is part of a lead structure, changing the stereochemistry or incorporating unnatural amino acids can help to decrease enzymatic hydrolysis.¹⁶ The switch from the naturally occurring amino acid L-valine to D-valine (**25**) caused a 100-fold drop of the inhibition potency toward MMP-13 (Table 3). The same effect could be observed for the enantiomeric pairs **26** vs. **27** and **28** vs. **29**, and changing the stereochemistry of the cyclohexyl and *tert*-butyl containing amino acid resulted in a decrease of IC_{50} values for MMP-13 (4.4 vs. 159 nM for cyclohexyl and 2.4 vs. 289 nM for *tert*-butyl). The selectivity amongst MMP-1, MMP-2, MMP-8, MMP-9, and MT1-MMP was the same for **25-27** and none of these compounds inhibited the remaining collagenases at the highest concentration tested (5 μM). In contrast, compound **28** showed low nanomolar inhibition of MMP-8 (IC_{50} = 17 nM). The tetrahydropyran containing compound **30**, possessing high inhibition potency for MMP-13 (IC_{50} = 1.9 nM), showed increased stability in human liver microsomes compared to the cyclohexyl containing compound (**26**). However, the selectivity of **30** for MMP-13 over MMP-8 (IC_{50} = 113 nM) is only ca. 50-fold. Compound **31**, which incorporated a cyclopropyl moiety, showed a highly increased *in vitro* half-life in mouse and human liver microsomes (31 and 74 min, respectively) compared to **2** and ca. 500- and 100-fold selectivity for MMP-13 vs. MMP-2 and MMP-8, respectively. All compounds except **25** (<40%) and **33** (<10%) inhibited collagen cleavage with >90% at an inhibitor concentration of 20 μM (Table 3).

Variation of the phenyl-furan unit of compound 2.

Next studied was the variation of the phenyl-furan biaryl unit in **2**. First, the synthesis of suitable building blocks containing different heterocycles was needed (Scheme 3). The phenyl- thiazole (**37**) and phenyl-oxazole (**41**) linkers were synthesized in the same way: a Suzuki reaction was followed by a radical benzylic bromination reaction using *N*-bromosuccinimide and benzoyl peroxide as the radical initiator to give the desired products. The imidazol-phenyl linker **44** was isolated after a three-step sequence: the methyl-imidazole derivative **42** was brominated, coupled with (4-(hydroxymethyl)phenyl)-boronic acid, and finally a benzylic bromination gave the desired product **44**. The three-step sequence for the formation of the pyridine containing linkers **48** and **50** was initiated by the conversion of **45** into the corresponding boronic acid pinacol ester **46** using $\text{Pd}(\text{dppf})_2$ as the

catalyst. Again, a Suzuki reaction was followed by a benzylic bromination reaction to yield **48** and **50**.

The five compounds **37**, **41**, **44**, **48**, and **50** were coupled with thiopyrimidone **6** under basic conditions before the ester moiety was hydrolyzed and the valine derivative **51** was added via amide bond formation using EDC as the coupling reagent to give compounds **52-56** (Scheme 4 and Table 4).

The furan ring in **2** was replaced by different five-membered heterocycles to minimize the potential toxicity and metabolizing liability of the electron rich furan heterocycle,²⁴ which can be easily oxidized and degraded by enzymes of the CYP450 family.²⁵ Compounds **52**, **53**, and **54** showed low nanomolar IC₅₀s (7.1, 18.1, and 37.5 nM, respectively) as well as high selectivity among the collagenases MMP-1, MMP-2, MMP-8, MMP-9, and MT1-MMP (Table 4). Among the three compounds **54** exhibited an excellent half-life (96 min) in human liver microsomes, but unfortunately only **52** inhibited collagen cleavage with >90% at an inhibitor concentration of 20 μM. Further assessment via a dose-responsive assay showed that **52** inhibited collagen cleavage with a 14.9 nM IC₅₀.

Substitution of the carbon-sulfur linker of compound **2**.

As the sulfur atom of the thiopyrimidone component of **2** could be easily oxidized *in vivo*, we designed a new set of compounds focusing on blocking the possible metabolically labile site by replacing the sulfur with either with a nitrogen, oxygen, or a carbon atom (Scheme 5A-C). 4-Bromo-2-fluorobenzeneacetic acid (**57**) was reduced to the corresponding homo-benzylic alcohol and the boronic acid pinacol ester was introduced via a palladium catalyzed cross-coupling reaction to give compound **58**. A Suzuki coupling was followed by a three-step sequence to install the amidine moiety in **60** before a condensation reaction with ethyl-2-oxocyclopentane-1-carboxylate completed the synthesis of methyl-ester **61** (Scheme 5A).

4-Bromo-2-fluorobenzylamine (**62**) was Boc-protected and the boronic acid pinacol ester was installed *via* a cross-coupling reaction using Pd(dppf)Cl₂ as the metal catalyst. A Suzuki reaction followed by Boc-deprotection provided primary amine **65** and finally, the pyrimidone group was added under basic conditions to give methyl ester **67** (Scheme 5B).

4-Bromo-2-fluorobenzyl alcohol (**68**) was converted into the boronic acid pinacol ester and coupled with methyl-5-bromofuran-2-carboxylate to give intermediate **69**, which was then exposed to triphenylphosphine and tetrabromomethane to provide the corresponding benzyl bromide, and the thiopyrimidone moiety was added via a substitution reaction using **70** as the nucleophile (Scheme 5C). After the methyl esters in **61**, **67**, and **71** were hydrolyzed, an amino acid coupling finished the syntheses of **72-74** (Scheme 6 and Table 5).

Interestingly, the potency dropped by 3-fold from the nitrogen containing compound (**72**, IC₅₀ = 5.5 nM) to the carbon atom containing inhibitor (**73**, IC₅₀ = 18.7 nM) and even 100-fold for the replacement of the sulfur atom in **2** with an oxygen atom (**76**, IC₅₀ = 697 nM) (Table 5). All three compounds showed an excellent selectivity profile among the remaining collagenases (MMP-1, MMP-2, MMP-8, MMP-9, and MT1-MMP) with IC₅₀ values higher

than 5 μM for all enzymes tested. The newly introduced nitrogen atom in **72** reduced the clogP and $\text{clogD}_{7.4}$ values (2.4 and 3.0, respectively) and increased the microsomal stability in human and rat liver microsomes to 17 and 22 min, respectively. Substitution of the sulfur atom by a CH_2 group doubled the human microsomal half-life (26 min) compared to **2**. Compounds **72** and **73** inhibited collagen cleavage greater than 95% at 20 μM , while **74** was not active in inhibiting collagen cleavage by MMP-13.

Variation of the pyrimidinone scaffold.

The next compound set was focused on variation of the cyclopentene ring of **2**, binding in the S_1' subsite. Potentially, the CH_2 groups could be easily accessible to metabolizing enzymes in the liver and could contribute to the moderate metabolic stability of **2**. The thiopyrimidinone building blocks **75-79** were commercially available and six more (**82**, **84**, **86**, **89**, **90** and **94**) were synthesized (Scheme 7). A condensation reaction of thiourea and ethyl-2-cyano-4,4-diethoxybutyrate followed by hydrolysis of the diethyl acetal under acidic conditions gave **80** in excellent yield. Treatment of **83** and **85** with sodium hydroxide gave the corresponding chloro-pyrimidinones **84** and **86**. Aminothiophene **87** was converted into the thiourea derivative **88** using amino thiocyanate and benzoyl chloride before refluxing in ethanolic KOH gave the desired thiopyrimidinone intermediates **89** and **90**.²⁶ Finally, the last thiopyrimidinone building block **94** was synthesized in a three-step sequence, whereby 2-amino-5-fluorobenzoic acid **91** was converted into the thiourea derivative **92** by using ethoxycarbonyl isothiocyanate under refluxing conditions, activation of the acid with acetic anhydride enabled nucleophilic attack and closure of the thiopyrimidinone ring to give **93**, and removal of the ethyl carbamate under basic conditions resulted in the isolation of **94** in good yield.

The coupling with the thio- and chloro-pyrimidinone fragments **96** and **97** proceeded *via* treatment with triethylamine and Huenig's base, respectively, to afford **98**. Subsequent ester hydrolysis followed by an amino acid coupling reaction provided compounds **99-110** (Scheme 8 and Table 6).

The substitution of the cyclopentene ring with a benzene (**99**) or a fluoro-benzene ring (**100**) gave two highly potent MMP-13 inhibitors ($\text{IC}_{50} = 9.4$ and 6.6 nM, respectively). Both compounds showed a good selectivity profile among the collagenases (MMP-1, MMP-2, MMP-8, MMP-9 and MT1-MMP) with only moderate activity for MMP-8 ($\text{IC}_{50} = 400$ and 270 nM, respectively). Additionally, the stability of **100** in human and rat liver microsomes dropped to 8 and 4 min, respectively, presumably due to increased lipophilicity ($\text{clogD}_{7.4} = 4.8$ and $\text{clogP} = 3.8$) of the compound compared to **2**. The incorporation of a thiophene ring resulted **101** and **102**, which were active MMP-13 inhibitors but only moderately inhibited collagen cleavage at an inhibitor concentration of 20 μM (77% and 51%, respectively). The potency of the pyrrole containing compounds **103** and **104** decreased significantly; compound **103** was not active at the highest concentration tested (5 μM) and **104** exhibited an IC_{50} value for MMP-13 of 2 μM . The pyrazole derivative of **2** (**105**) also lost potency against MMP-13 ($\text{IC}_{50} = 274$ nM). Removing the cyclopentene ring completely (**106**) or substituting the thiopyrimidinone ring with a fluorine atom (**107**) or a trifluoromethyl group (**110**) also resulted in a decrease of activity towards MMP-13 ($\text{IC}_{50} = 153$ nM, 2.6 μM , and

1.2 μM , respectively), although **106** and **110** showed excellent stability especially in human liver microsomes (>120 min for both compounds). These data supported our hypothesis that the saturated carbon atoms in the thiopyrimidone part of **2** are metabolically labile sites and easily accessible for hepatic oxidation.

After the comparison and analysis of the *in vitro* properties of the compounds described herein, seven were selected for further evaluation of their permeability and solubility properties (Table 7). Inhibitors **21**, **22**, and **23** were part of the first compound set, which was focused on the variation of the terminal methylamine group in **2**. The three compounds have an excellent selectivity profile within the collagenases (IC_{50} values for MMP-1, MMP-2, MMP-8, MMP-9, and MT1-MMP >5 μM) and all three have improved half-lives in rat liver microsomes (72, 29, and 25 min, respectively) compared with **2**. A special focus has been placed on the *in vitro* hepatic stability in rats as further *in vivo* PK is planned to be performed in rats. Compounds **31** and **28** possessed unnatural amino acids, which could protect these compounds from proteolytic cleavage *in vivo*. Compound **52** does not exhibit improved microsomal half-life but is lacking the furan ring from **2** which has been attributed to toxicity for other compounds in preclinical studies.^{24, 27} Finally, compound **72**, in which the metabolically labile sulfur was replaced by a nitrogen atom, exhibited good microsomal stability in rat liver microsomes (22 min) and had significantly reduced $\text{clogD}_{7.4}$ and clogP values (3.0 and 2.4, respectively), which contribute to improved solubility properties.

The artificial membrane permeability assay (PAMPA assay)¹⁵ is a rapid, low-cost, fast, and high-throughput *in vitro* method to assess the gastrointestinal permeability properties of a compound. The passive diffusion of a potential drug through a phospholipid bilayer can be monitored to obtain *in vivo* permeability insights. The permeability in the PAMPA assay for the compounds **21** (3.4 nm/s) and **23** (0.3 nm/s) was extremely low. Compound **21**, which exhibits clogP and $\text{clogD}_{7.4}$ values of 4.1 and 5.1, respectively, shows 61% retention and is too lipophilic to pass the lipid bilayer. On the other hand the retention of compound **23** is lower (30%) but presumably the secondary amine within the azetidine ring is protonated under the weakly acidic conditions used in the PAMPA assay mimicing the pH in the intestine, which restricts the compound from diffusing through the lipid bilayer.

The two best compounds which exhibited low retention ($<30\%$), good permeability (ca. 20 nm/s), and good kinetic solubility (> 15 μM) were **28** and **31** (17%, 72.9 nm/s, and 16.0 μM for **28** and 24%, 19.1 nm/s, and 47.5 μM for **31**, respectively).

***In vivo* PK properties.**

For a first assessment of the *in vivo* stability of the synthesized MMP-13 inhibitors, compounds **2**, **28** and **30-32** were subjected to PK analysis after IV administration (1 mg/kg dose; Table 8) in rats. Lead compound **2** provided a reference, but as our future goal is to develop an orally bioavailable MMP-13 inhibitor, we focused on compounds **28** and **30-32** as the substitution of L-valine in **2** by unnatural amino acids should minimize possible cleavage by peptidases and proteases in the gastrointestinal tract. Compounds **28**, **30** and **32** did not show the best selectivity profiles within the different MMPs tested but compound **28** exhibited excellent permeability (72.9 nm/s) in the PAMPA assay as well as reasonable

solubility (16 μM). Compounds **30** and **32** were selected for further evaluation in *in vivo* PK studies due to their increased stabilities in human liver microsomes (29 and 59 min, respectively). There was not much difference in the rat *in vivo* PK parameters after IV dosing for the five compounds but all of them exhibited excellent plasma half-lives (> 2.4 h), reached maximum concentrations higher than 50 μM , and had very low clearance rates with less than 0.3 mL/min/kg. Furthermore, the concentration of **2** in the synovial fluid of the rat knee after IP injection was evaluated to determine if the inhibitor was reaching its needed place of action. At the 4 h time point the concentration of **2** in the synovial fluid was 380 nM, which is ca. 140 times higher than its IC_{50} for MMP-13.

CYP inhibition.

The inhibition of cytochrome P450 isoforms, especially CYP 3A4, can be a major drawback in drug development, potentially indicating toxicity. CYP 3A4 inhibition has also been responsible for the termination of the development of MMP-13 inhibitors.²⁸ Therefore, we further assessed the *in vitro* inhibition of CYP 1A2, 2C9, 2D6, and 3A4 for the compounds **2**, **28** and **30-32** (Table 9) at a concentration of 10 μM . The lead compound **2** inhibited CYP 2C9 and 3A4 at levels of 60 and 16%, respectively. Interestingly, compound **28** inhibited CYP 2C9 and 3A4 even more strongly, 75 and 43%, respectively. Compounds **30**, **31**, and **32** exhibited lower inhibition of CYP 2C9 (35, 29, and 25%, respectively) and did not inhibit the activity of CYP 3A4.

Molecular Modeling.

Docking studies were performed to rationalize potency trends within the SAR study of our MMP-13 inhibitors. In particular, we investigated the lack of discrimination of inhibition potency between the enantiomeric pairs **9/10**, **11/12**, **13/14**, and **15/16** (Table 2), in contrast to **2/25**, **26/27**, **28/29** (Table 3). We have already demonstrated that a combination of hydrophobic interactions of the isopropyl group and hydrogen bonding interactions between the amide group in compound **2** with the backbone amide groups of Gly183 and Tyr244 in MMP-13 is responsible for a 40-fold higher inhibition potency compared to its enantiomeric counterpart.¹³ A similar trend is observed for the enantiomeric pairs **26/27** and **28/29**, respectively, which possess hydrophobic groups in their R positions (Table 3). However, in **9/10**, **11/12**, **13/14**, and **15/16**, where the terminal methyl group of **2** is substituted by hydrophilic moieties (R1-groups, Table 2), which are able to form additional hydrogen bonding interactions with Tyr214 and/or Ser182 as shown in our docking models (Figure 3A-D), an analogous drop in inhibition potency was not observed. We surmised from these observations that the hydrophobic contact between the isopropyl unit and Ile243 is less significant than the additional hydrogen bonding interactions by the polar R₁-groups. Alternatively, the (*R*)-enantiomers could bind to MMP-13 in the same binding pose as (*R*)-**2** in the X-ray co-crystal structure (PDB code: 5UWM).¹³ In this binding mode (Figures 3E, 3F), the polar R1-groups can form hydrogen bonding interactions with Glu223 or backbone amides of MMP-13, and the loss of hydrogen bonds of the amide units of the (*R*)-enantiomers can be compensated by the polar interactions of the corresponding R1- group. Consequently, the enantiomeric pairs **9/10**, **11/12**, **13/14**, and **15/16** exhibit high inhibition potency regardless of their stereoconfiguration.

We also performed docking studies to examine the preference of the sulfur linkage (**2**) vs. nitrogen (**72**), carbon (**73**), or oxygen (**74**) linkages (Table 5) in terms of inhibition potency. We assume that due to the smaller dihedral angle for C_{sp2}-S-C_{sp3} (101.5°, **2**) compared to those for C_{sp2}-N-C_{sp3} (119.3°, **72**), C_{sp2}-C-C_{sp3} (114.4°, **73**), and C_{sp2}-O-C_{sp3} (117.3°, **74**), respectively, the cyclopentyl unit in compound **2** is aligned in an optimal position for forming hydrophobic contacts with the protein surface composed of Phe252, Pro255, and Leu239 (Supporting Fig S1 A). Furthermore, the increased dihedral angles in **72**, **73**, and **74** lead to a slightly deviated alignment of the carbonyl oxygen within the pyrimidinone part of the structures, which results in a less favorable orientation for the formation of hydrogen bonding interactions with Thr247 and explains the decreased inhibition of MMP-13. Interestingly, compound **72** has the largest dihedral angle, which should lead to the least favorable orientation for the formation of hydrogen bonding interaction as well as hydrophobic contacts, but an additional hydrogen bond by the hydrogen atom of the amine linkage with Thr245 might be the reason which compensates the drop in inhibition potency to only twofold compared to compound **2**. (Supporting Fig S1B).

The significance of the hydrophobic contact between the cyclopentyl unit in **2** and the hydrophobic surface of MMP-13 is also reflected within the SAR of the compounds shown in Table 6. The compounds **106**, **107**, **108**, **109**, and **110**, which are lacking the cyclopentyl moiety and can not form hydrophobic contacts, exhibit decreased inhibition potency by 30 ~ 1,000 fold compared to **2**, while **99**, **100**, **101**, and **102** have similar IC₅₀ values as compound **2**.

We also investigated the replacement of the furan ring in compound **2** with other heterocycles (Table 4) by docking studies. The central part of the structures **2**, **52**, **53**, **54**, **55**, and **56**, comprising the phenyl ring connected to the corresponding 5- membered heterocycles, occupies the same area within the binding site of MMP-13 with high alignment to each other. However, the methyl group attached to the imidazole ring in **53** causes a non-planar conformation of the amide unit connected to the imidazole ring with a dihedral angle of 34.5°. This non-planar conformation results in the loss of hydrogen bond interaction between the N-methylamide unit of **53** and the amide backbone of Tyr244, and might be responsible for a decreased inhibition of MMP-13 (Supporting Fig s2a, B).

Conclusions.

Starting from compound **2** a comprehensive SAR/SPR study was performed by systematically varying all five subunits (Figure 2). As a goal of this study, we were interested in finding a set of selective and potent MMP-13 inhibitors that can be used in *in vivo* efficacy studies in a rat OA model. Analogs of **2** were designed and synthesized to investigate their SAR/SPR in terms of inhibition potency, specificity, microsomal stability, solubility, and permeability. As hepatic metabolization is a significant challenge in drug discovery, we focused on the optimization of the *in vitro* microsomal stability at the beginning of the lead optimization process. We found that substituting the terminal methyl group of **2** with cyclohexanol (compound **21**) gave a highly selective MMP-13 inhibitor with increased *in vitro* microsomal stabilities in rats and mice but the hepatic stability in humans was not improved compared to **2**. The addition of small saturated heterocycles such as an

oxetane (**22**) or azetidine ring (**23**) gave potent and selective MMP-13 inhibitors with increased microsomal stabilities in human liver microsomes. The variation of the amino acid part of **2** provided three compounds (**30-32**) with very promising human microsomal stabilities ($t_{1/2} = 29, 74, \text{ and } 59 \text{ min}$, respectively). Out of these three compounds only **31** showed a good selectivity profile within the collagenases; inhibition of MMP-8 resulted in an IC_{50} value of 832 nM, which was a 100-fold worse compared with MMP-13.

Displacement of the furan-phenyl ring system with other heterocyclic rings gave highly active compounds with increased human microsomal stabilities (Table 4). However, only **52** was able to inhibit collagen cleavage at a concentration of 20 μM , while all other compounds inhibited the cleavage of the natural substrate by less than 30%. Substitution of the sulfur atom within the thiopyrimidone scaffold of **2** with a nitrogen (**72**) or carbon (**73**) atom improved the human microsomal half-life (17 and 26 min, respectively). This result suggested that the sulfur atom could be oxidized by human hepatic metabolizing enzymes. Finally, the removal of the saturated carbon atoms within the S_1 'subsite binding thiopyrimidone scaffold enhanced metabolic stability, as compound **106** showed greatly improved microsomal stabilities (rat/mouse/human 33/57/160 min) compared to **2**. Unfortunately, removal of the CH_2 -groups resulted in a loss of activity (**106-110**) and/or selectivity (**99** and **100**).

After testing the solubility and permeability of a selected compound set (Table 7) we identified compound **31** which exhibited improved microsomal half-life times (human/rat/mouse 74/13/31 min). Although the permeability coefficient for **31** (21.1 nm/s) is in the same range as for compound **2**, its retention within the artificial phospholipid bilayer in the PAMPA assay is lower (24% for **31** versus 47% for **2**) and the kinetic solubility is improved by three-fold. Furthermore, compound **31** shows no inhibition of CYP 3A4 and exhibited excellent *in vivo* PK properties after IV dosing. As **31** is structurally closely related to **2** which could be detected in the synovial fluid at a concentration of 380 nM, we expect **31** to show a similar distribution into the rat knee. Therefore, considering the improved pharmacokinetic properties, compound **31** appears to be an appropriate candidate for a first round of *in vivo* efficacy studies in a rat OA model (Table 10). Additionally, combining the best results observed here for each subunit modification, i.e. (**22** or **23**) and (**28** or **31**) and (**72** or **73**), may provide improved compounds for *in vivo* use.

Recent studies have produced a variety of selective MMP-13 inhibitors.²⁹ However, distinct drawbacks to these inhibitors have been reported. For inhibitors presented as organic anions, binding to human organic anion transporter 3 resulted in nephrotoxicity.³⁰ Inhibitors possessing carboxylic acids may generate reactive metabolites through protein conjugation of the resulting acyl glucuronide.^{30,31} Pyrimidine-2-carboxamide-4-one-based inhibitors have exhibited poor bioavailability, low volume of distribution, poor metabolic stability, and/or P450 3A4 inhibition.²⁸ Obtaining appropriate kinetic solubilities for MMP-13 inhibitors has proved challenging.^{12, 32} Due to design considerations based on activity profiles and prior data, several of the compounds described herein avoid many of these pitfalls, particularly poor solubility and metabolic stability as well as the potential for nephrotoxicity and generation of reactive metabolites.

Supplementary Material

Refer to Web version on PubMed Central for supplementary material.

Acknowledgments

This research was supported by NIH R01 grant AR063795 (GBF and WRR). RF was supported by a Schroedinger Postdoctoral Fellowship, financed by the Austrian Science Fund (FWF).

References

- Chen A, Gupte C, Akhtar K, Smith P, Cobb J. The global economic cost of osteoarthritis: How the UK compares. *Arthritis*. 2012; D01:10.1155/2012/698709.
- Lee AS, Ellman MB, Yan D, Kroin JS, Cole BJ, Van Wijnen AJ, Im HJ. A current review of molecular mechanisms regarding osteoarthritis and pain. *Gene*. 2013;527:440–447. [PubMed: 23830938]
- Bijlsma JWJ, Berenbaum F, Lafeber PJG. Osteoarthritis: an update with relevance for clinical practice. *The Lancet* 2011;377:2115–2126.
- (a) Flood J The role of acetaminophen in the treatment of osteoarthritis. *Am. J. Manag. Care* 2010;16:48–54;(b) Chen YF, Jobanputra P, Barton P, Bryan S, Fry-Smith A, Harris G, Taylor RS Cyclooxygenase-2 selective non-steroidal anti-inflammatory drugs (etodolac, meloxicam, celecoxib, rofecoxib, etoricoxib, valdecoxib and lumiracoxib) for osteoarthritis and rheumatoid arthritis: a systematic review and economic evaluation. *Health Technol. Asses.* 2008;12:1–278.
- Aigner T, Sachse A, Gebhard PM, Roach HI. Osteoarthritis: Pathobiology—targets and ways for therapeutic intervention. *Adv. Drug Deliver. Rev.* 2006;58:128–149.
- Mengshol JA, Mix KS, Brinckerhoff CE. Matrix metalloproteinases as therapeutic targets in arthritic diseases: Bull’s-eye or missing the mark? *Arthritis Rheum.* 2002;46:13–20. [PubMed: 11817584]
- (a) Takaishi H, Kimura T, Dalal S, Okada Y, D’Armiento J. Joint diseases and matrix metalloproteinases: A role for MMP-13. *Curr. Pharm. Biotechnol.* 2008;9:47–54; [PubMed: 18289056] (b) Neuhold LA, Killar L, Zhao WG, Sung MLA, Warner L, Kulik J, Turner J, Wu W, Billinghamurst C, Meijers T, Poole AR, Babij P, DeGennaro LJ. Postnatal expression in hyaline cartilage of constitutively active human collagenase-3 (MMP-13) induces osteoarthritis in mice. *J. Clin. Invest.* 2001;107:35–44. [PubMed: 11134178]
- (a) Burrage PS, Mix KS, Brinckerhoff CE. Matrix metalloproteinases: Role in arthritis. *Front. Biosci.* 2006;11:529–543; [PubMed: 16146751] (b) Fingleton B. MMPs as therapeutic targets—Still a viable option? *Semin. Cell Dev. Biol.* 2008;19:61–68. [PubMed: 17693104]
- (a) Chen JM, Nelson FC, Levin JI, Mobilio D, Moy FJ, Nilakantan R, Zask A, Powers R. Structure-based design of a novel, potent, and selective inhibitor for MMP-13 utilizing NMR spectroscopy and computer-aided molecular design. *J. Am. Chem. Soc.* 2000;122:9648–9654;(b) Engel CK, Pirard B, Schimanski S, Kirsch R, Habermann J, Klingler O, Schlotte V, Weithmann KU, Wendt KU. Structural basis for the highly selective inhibition of MMP-13. *Chemistry & Biology* 2005;12:181–189; [PubMed: 15734645] (c) Reiter LA, Freeman-Cook KD, Jones CS, Martinelli GJ, Antipas AS, Berliner MA, Datta K, Downs JT, Eskra JD, Forman MD, Greer EM, Guzman R, Hardink JR, Janat F, Keene NF, Laird ER, Liras JL, Lopresti- Morrow LL, Mitchell PG, Pandit J, Robertson D, Sperger D, Vaughn-Bowser ML, Waller DM, Yocum SA. Potent, selective pyrimidinetrione-based inhibitors of MMP-13. *Bioorg. Med. Chem. Lett.* 2006;16:5822–5826; [PubMed: 16942871] (d) Johnson AR, Pavlovsky AG, Ortwine DF, Prior F, Man CF, Bornemeier DA, Banotai CA, Mueller WT, McConnell P, Yan C, Baragi V, Lesch C, Roark WH, Wilson M, Datta K, Guzman R, Han HK, Dyer RD. Discovery and characterization of a novel inhibitor of matrix metalloproteinase-13 that reduces cartilage damage in vivo without joint fibroplasia side effects. *J. Biol. Chem.* 2007;282:27781–27791; [PubMed: 17623656] (e) Gooljarsingh LT, Lakdawala A, Coppo F, Luo L, Fields GB, Tummino PJ, Gontarek RR. Characterization of an exosite binding inhibitor of matrix metalloproteinase 13. *Protein Sci.* 2008;17:66–71; [PubMed: 18042679] (f) Li JJ, Nahra J, Johnson AR, Bunker A, O’Brien P, Yue WS, Ortwine DF, Man CF, Baragi V, Kilgore K, Dyer RD, Han HK. Quinazolinones and pyrido[3,4-d]pyrimidin-4-ones as

- orally active and specific matrix metalloproteinase-13 inhibitors for the treatment of osteoarthritis. *J. Med. Chem.* 2008;51:835–841; [PubMed: 18251495] (g) Heim-Riether A, Taylor SJ, Liang S, Gao DA, Xiong Z, Michael August E, Collins BK, Farmer Ii BT, Haverty K, Hill-Drzewi M, Junker HD, Mariana Margarit S, Moss N, Neumann T, Proudfoot JR, Keenan LS, Sekul R, Zhang Q, Li J, Farrow NA. Improving potency and selectivity of a new class of non-Zn-chelating MMP-13 inhibitors. *Bioorg. Med. Chem. Lett.* 2009;19:5321–5324. [PubMed: 19692239]
10. (a) Nara H, Kaieda A, Sato K, Naito T, Mototani H, Oki H, Yamamoto Y, Kuno H, Santou T, Kanzaki N, Terauchi J, Uchikawa O, Kori M. Discovery of novel, highly potent, and selective matrix metalloproteinase (MMP)-13 inhibitors with a 1,2,4-triazol-3-yl moiety as a zinc binding group using a structure-based design approach. *J. Med. Chem.* 2017;60:608–626; [PubMed: 27966948] (b) Gege C, Bao B, Bluhm H, Boer J, Gallagher BM, Korniski B, Powers TS, Steeneck C, Taveras AG, Baragi VM. Discovery and evaluation of a non-Zn chelating, selective matrix metalloproteinase 13 (MMP-13) inhibitor for potential intra-articular Treatment of osteoarthritis. *J. Med. Chem.* 2011;55: 709–716.
 11. (a) Lauer-Fields JL, Minond D, Chase PS, Baillargeon PE, Saldanha SA, Stawikowska R, Hodder P, Fields GB. High throughput screening of potentially selective MMP-13 exosite inhibitors utilizing a triplehelical FRET substrate. *Bioorg. Med. Chem.* 2009;17:990–1005; [PubMed: 18358729] (b) Roth J, Minond D, Darout E, Liu Q, Lauer J, Hodder P, Fields GB, Roush WR. Identification of novel, exosite-binding matrix metalloproteinase-13 inhibitor scaffolds. *Bioorg. Med. Chem. Lett.* 2011;21:7180–7184. [PubMed: 22018790]
 12. Spicer TP, Jiang JW, Taylor AB, Choi JY, Hart PJ, Roush WR, Fields GB, Hodder PS, Minong D. Characterization of selective exosite-binding inhibitors of matrix metalloproteinase 13 that prevent articular cartilage degradation in vitro. *J. Med. Chem.* 2014;57:9598–9611. [PubMed: 25330343]
 13. Choi JY, Fuerst R, Knapinska AM, Taylor A, Smith L, Cao X, Hart PJ, Fields GB, Roush WR. Structure-based design and synthesis of potent and selective matrix metalloproteinase 13 inhibitors. *J. Med. Chem.* 2017;60:3814–3827. [PubMed: 28394608]
 14. (a) Fields GB. Interstitial collagen catabolism. *J. Biol. Chem.* 2013;288:8785–8793; [PubMed: 23430258] (b) Amar S, Smith L, Fields GB. Matrix metalloproteinase collagenolysis in health and disease. *Biochim. Biophys. Acta Mol. Cell Res.* 2017;1864:1940–1951. [PubMed: 28456643]
 15. Kansy M, Senner F, Gubernator K. Physicochemical high throughput screening: Parallel artificial membrane permeation assay in the description of passive absorption processes. *J. Med. Chem.* 1998;41:1007–1010. [PubMed: 9544199]
 16. Kerns EH, Di Li. *Drug-like Properties: Concepts, Structure, Design and Methods: From ADME to Toxicity Optimization.* Oxford, UK: Elsevier; 2008.
 17. Comer JEA. High-Throughput Measurement of logD and pKa In: Van de Waterbeemd H, Lennernäs H, Artursson P, eds. *Drug Bioavailability: Estimation of Solubility, Permeability, Absorption and Bioavailability.* Weinheim, D: Wiley-VCH Verlag GmbH & Co. KGaA; 2004:pp21–45.
 18. Madoux F, Li X, Chase P, Zastrow G, Cameron MD, Conkright JJ, Griffin PR, Thacher S, Hodder P. Potent, selective and cell penetrant Inhibitors of SF-1 by functional ultra-high-throughput screening. *Mol. Pharmacol.* 2008;73:1776–1784. [PubMed: 18334597]
 19. Obach RS. Prediction of human clearance of twenty-nine drugs from hepatic microsomal intrinsic clearance data: An examination of in vitro half-life approach and nonspecific binding to microsomes. *Drug Metab. Dispos.* 1999;27:1350–1359. [PubMed: 10534321]
 20. Van de Waterbeemd H, Smith DA, Beaumont K, Walker DK. Property-based design: Optimization of drug absorption and pharmacokinetics. *J. Med. Chem.* 2001;44:1313–1333. [PubMed: 11311053]
 21. Nassar AEF, Kamel AM, Clarimont C. Improving the decision making process in the structural modification of drug candidates: Enhancing metabolic stability. *Drug Discovery Today* 2004;9:1020–1028. [PubMed: 15574318]
 22. Lauer-Fields JL, Fields GB. Triple-helical peptide analysis of collagenolytic protease activity. *Biol. Chem.* 2002;383:1095–1105. [PubMed: 12437092]
 23. Hamman JH, Enslin GM, Kotze AF. Oral delivery of peptide drugs. *BioDrugs* 2005;19:165–177. [PubMed: 15984901]

24. Nelson SD. Metabolic activation and drug toxicity. *J. Med. Chem.* 1982;25:753–765. [PubMed: 7050382]
25. Zhou S, Chan SY, Goh BC, Chan E, Duan W, Huang M, McLeod HL. Mechanism-based inhibition of cytochrome P450 3A4 by therapeutic drugs. *Clin. Pharmacokinet.* 2005;44:279–304. [PubMed: 15762770]
26. Song YH, Son HY. Synthesis of New 1-Phenylthieno[1,2,4]triazolo[4,3-a]pyrimidin-5(4H)-one derivatives. *J. Heterocycl. Chem.* 2011;48:597–603.
27. Peterson LA. Electrophilic intermediates produced by bioactivation of furan. *Drug Metab. Rev.* 2006;38:615–626. [PubMed: 17145691]
28. Nara H, Sato K, Kaieda A, Oki H, Kuno H, Santou T, Kanzaki N, Terauchi J, Uchikawa O, Kori M. Design, synthesis, and biological activity of novel, potent, and highly selective fused pyrimidine-2-carboxamide-4-one-based matrix metalloproteinase (MMP)-13 zinc-binding inhibitors. *Bioorg. Med. Chem.* 2016;24:6149–6165. [PubMed: 27825552]
29. Xie XW, Wan RZ, Liu ZP. Recent research advances in selective matrix metalloproteinase-13 inhibitors as anti-osteoarthritis agents. *ChemMedChem* 2017;12:1157–1168. [PubMed: 28722301]
30. Ruminski PG, Massa M, Strohbach J, Hanau CE, Schmidt M, Scholten JA, Fletcher TR, Hamper BC, Carroll JN, Shieh HS, Caspers N, Collins B, Grapperhaus M, Palmquist KE, Collins J, Baldus JE, Hitchcock J, Kleine HP, Rogers MD, McDonald J, Munie GE, Messing DM, Portolan S, Whiteley LO, Sunyer T, Schnute ME. Discovery of N-(4-fluoro-3-methoxybenzyl)-6-(2-(((2S,5R)-5-(hydroxymethyl)-1,4-dioxan-2-yl)methyl)-2H-tetrazol-5-yl)-2-methylpyrimidine-4-carboxamide. A highly selective and orally bioavailable matrix metalloproteinase-13 inhibitor for the potential treatment of osteoarthritis. *J. Med. Chem.* 2016;59:313–327. [PubMed: 26653735]
31. Sallusti BC, Sabordo L, Evans AM, Nation RL. Hepatic disposition of electrophilic acyl glucuronide conjugates. *Curr. Drug Metab.* 2000;1:163–180. [PubMed: 11465081]
32. Nara H, Sato K, Naito T, Mototani H, Oki H, Yamamoto Y, Kuno H, Santou T, Kanzaki N, Terauchi J, Uchikawa O, Kori M. Thieno[2,3-d]pyrimidine-2-carboxamides bearing a carboxybenzene group at 5-position: Highly potent, selective, and orally available MMP-13 inhibitors interacting with the S1 “ binding site. *Bioorg. Med. Chem.* 2014;22:5487–5505. [PubMed: 25192810]

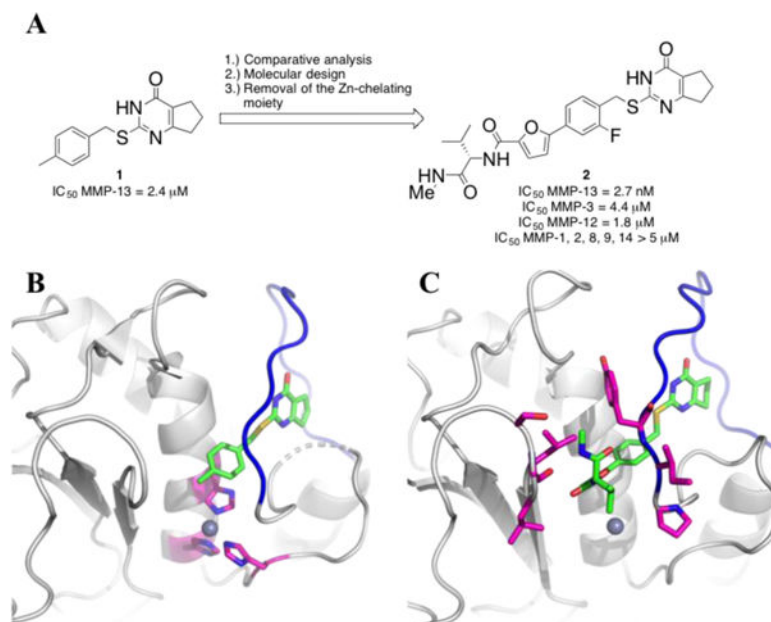


Figure 1.

(A) Hit to lead optimization of **2**. (B) The co-crystal structure of **1** with MMP-13 (PDB 4L19). Compound **1** is represented in green carbon sticks (red oxygen, blue nitrogen, and yellow sulfur), and hydrogen atoms are omitted for clarity. Three Zn-chelating His residues (His 222, His 226, and His 232) are represented in magenta carbon sticks. The S₁' specificity loop is shown as a blue tube. (C) The co-crystal structure of (*S*)-**2**¹³ with MMP-13 (PDB 5UWL). Compound **2** is represented in green carbon sticks. The S₁' specificity loop is shown as a blue tube. The amino acid side chains that can form direct interaction with parts of (*S*)-**2** (*N*-methylvaline-biaryl units) are shown as magenta sticks.

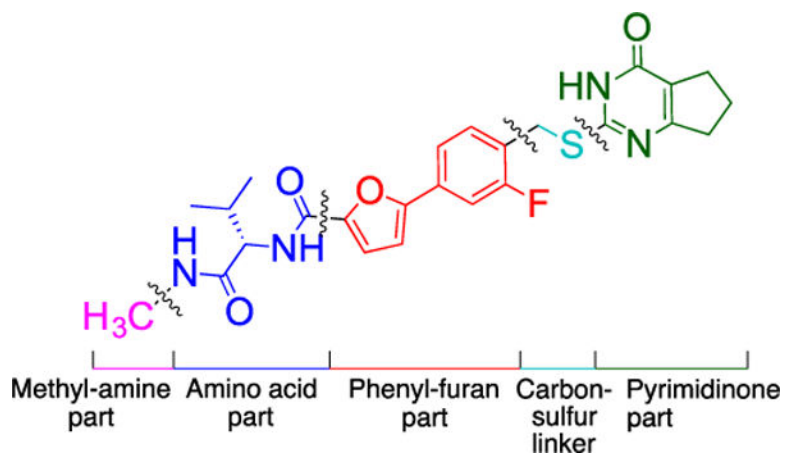


Figure 2.
The five subunits of compound 2.

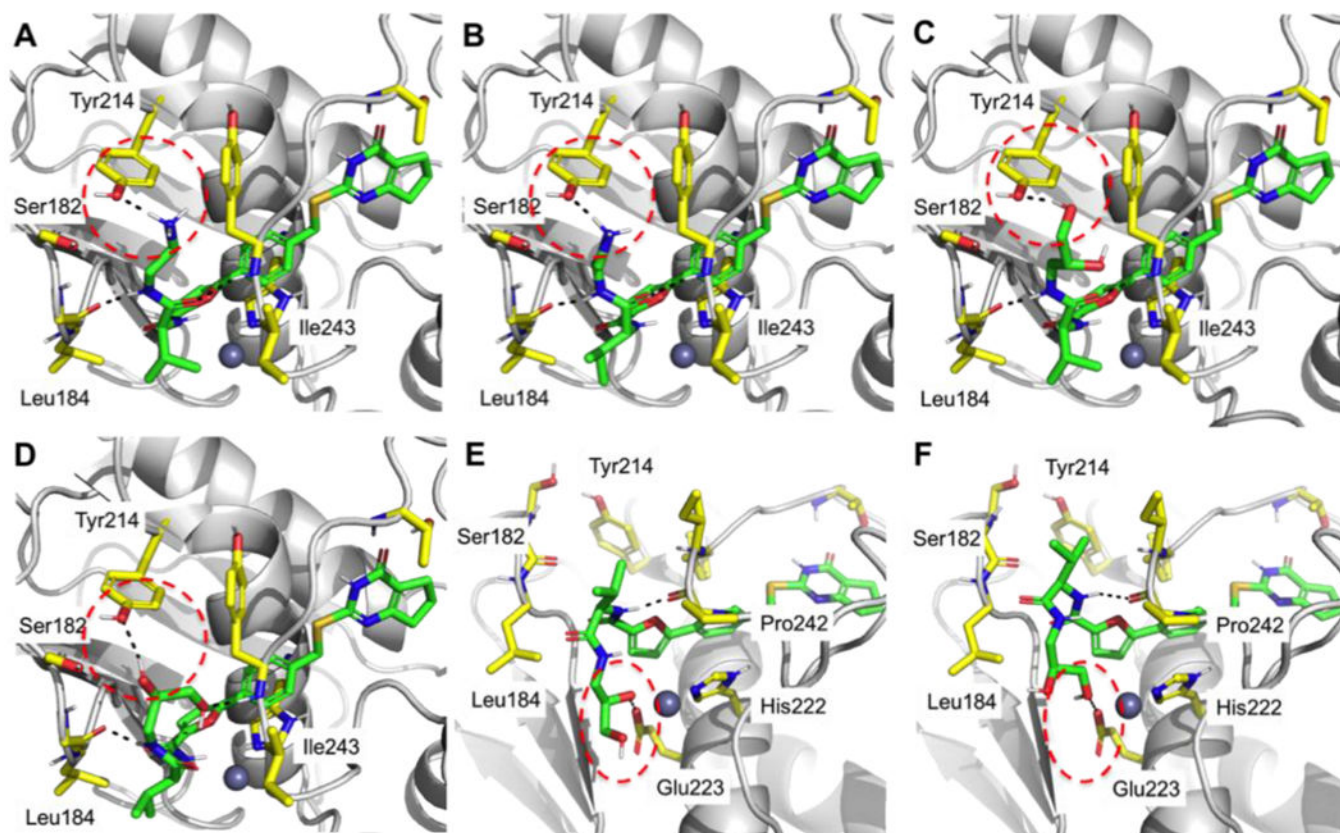
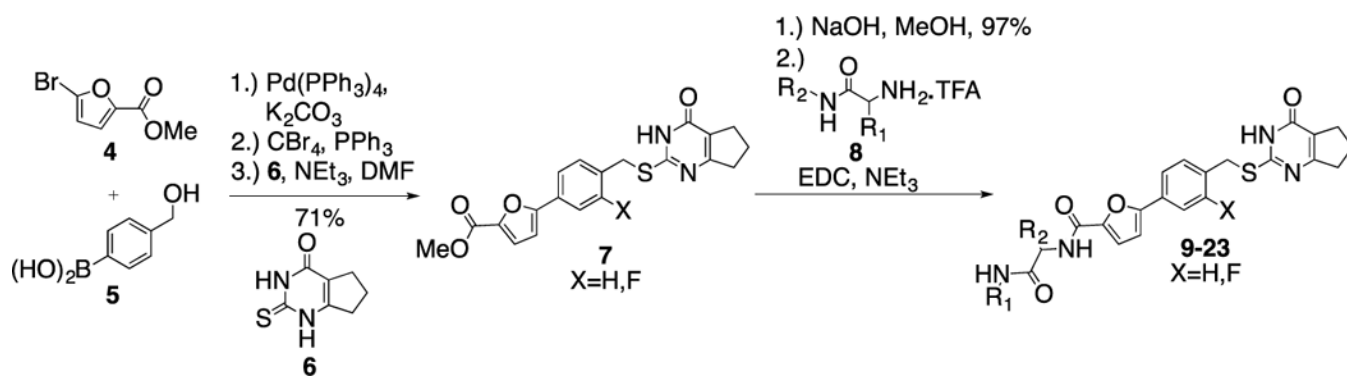
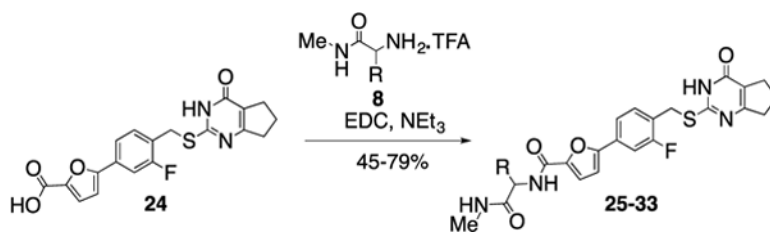
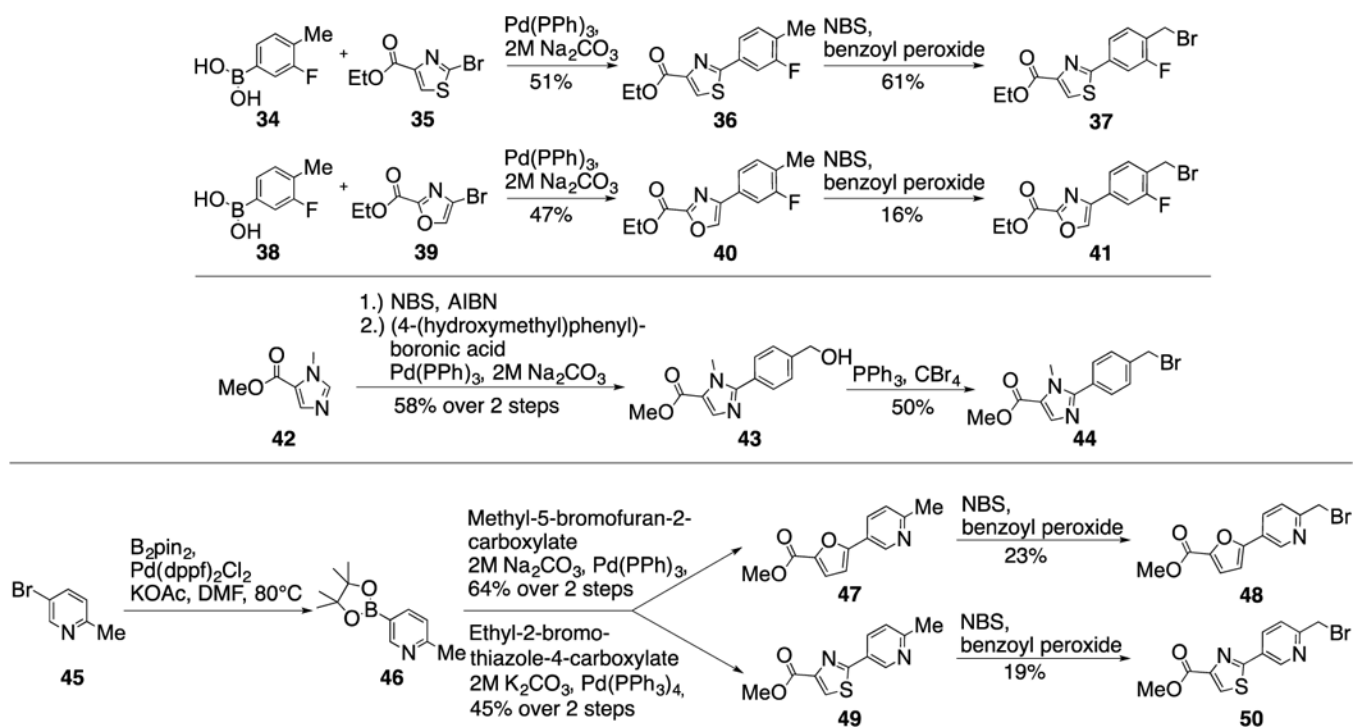


Figure 3. Predicted binding poses of compounds **9** (A), **10** (B), **11** (C), **12** (D,E), and **14** (F) in the active site of MMP-13. (E, F) Alternative binding poses of **12**, **14**, and other (*R*)-enantiomers. Ligand-protein interactions are shown in black dashed lines. Hydrogen bond interactions are marked with a red dashed circle. Inhibitors are presented in green sticks, and amino acids near inhibitors are in yellow sticks. Pymol was used to generate figures.

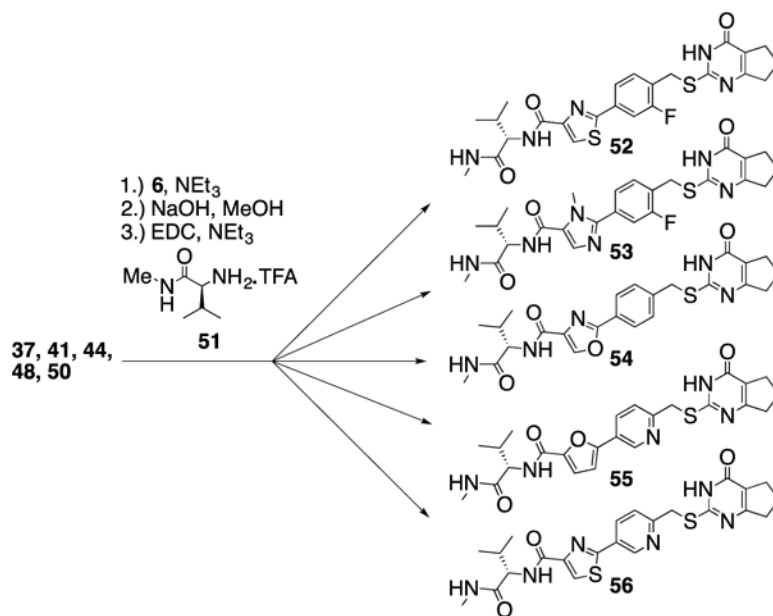
**Scheme 1.**Synthesis of compounds with variation of the terminal methylamine unit of **2**.



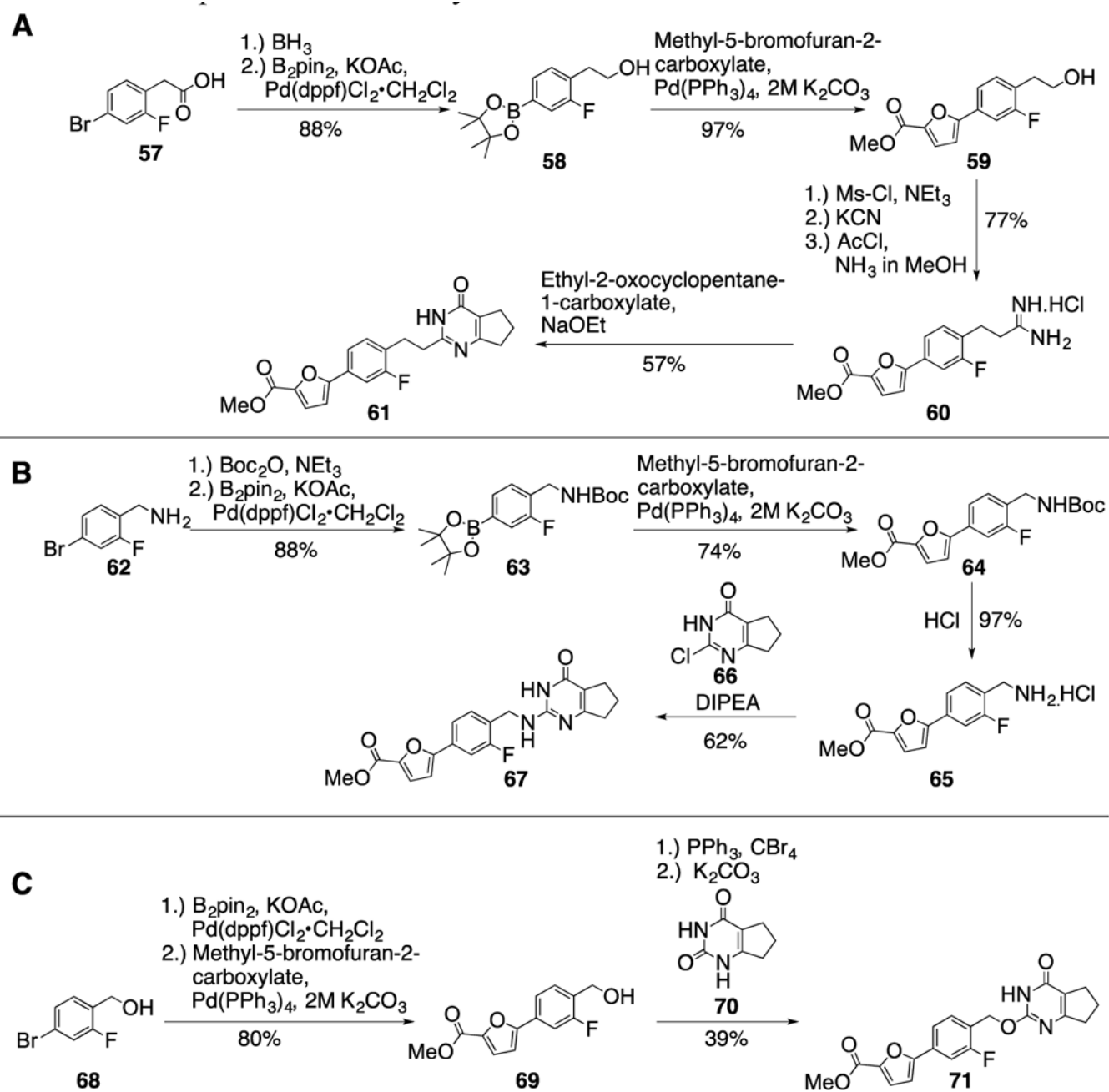
Scheme 2.
Synthesis of compounds with variation of the amino acid component of 2.



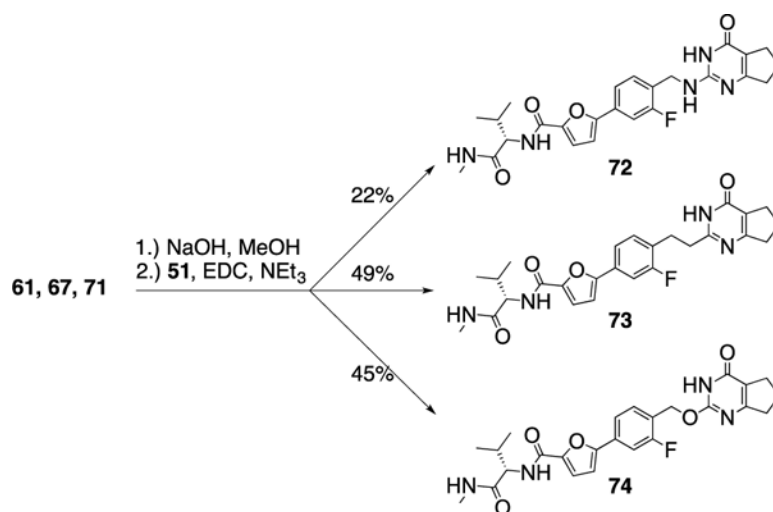
Scheme 3.
Synthesis of building blocks containing different heterocycles.



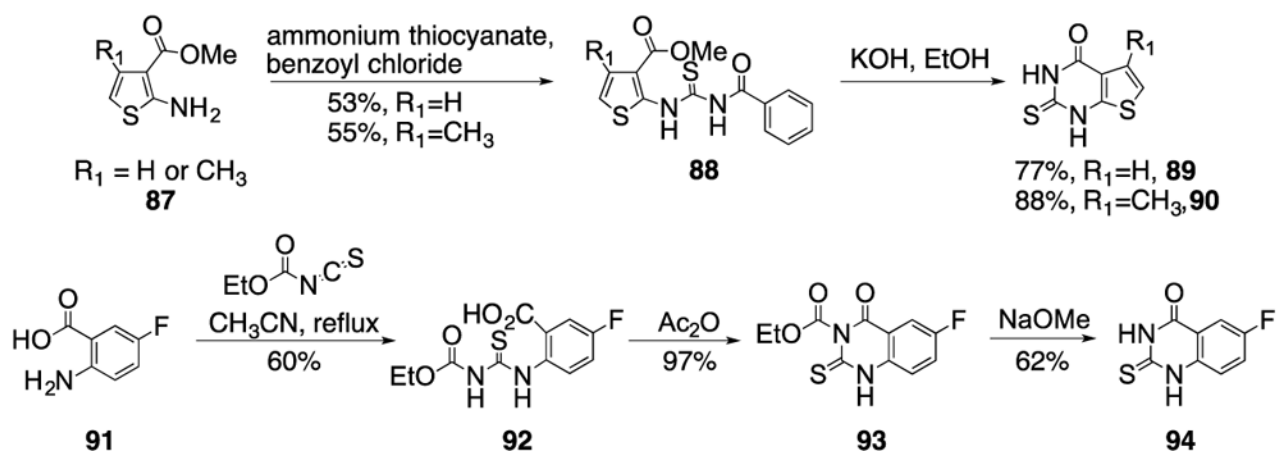
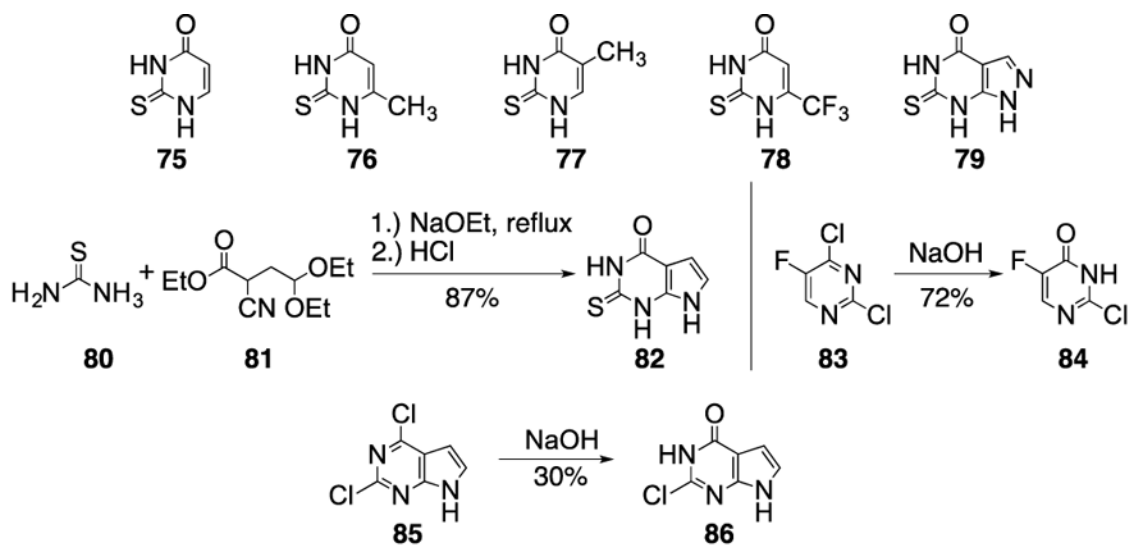
Scheme 4.
Replacement of the phenyl-furan linker in **2**.



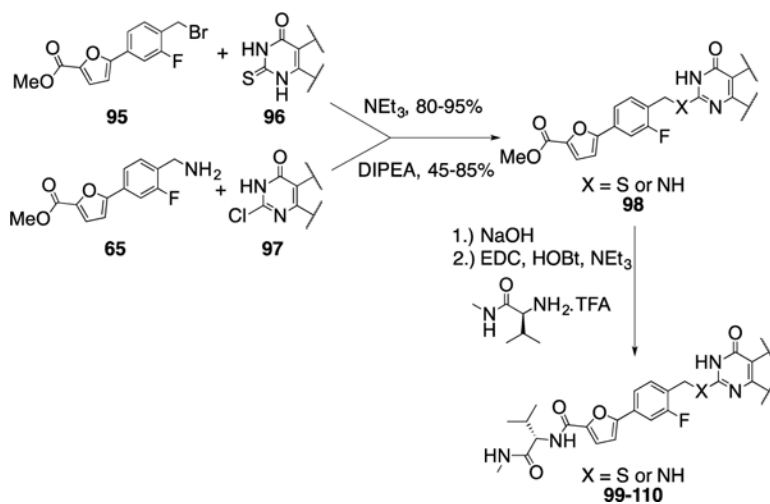
Scheme 5.
Synthesis of intermediates replacing the sulfur atom of compound 2.



Scheme 6.
Synthesis of **72-74**; replacing the sulfur atom of compound **2**.



Scheme 7.
Structures and synthesis of thiopyrimidinone building blocks.



Scheme 8.
Synthesis of compounds **99–110**. Compound **95** was previously described.¹³

Table 1.Physicochemical and *in vitro* PK properties of **2**.

Property	Compound 2
clogD _{7.4} ^a	4.2
clogP ^b	3.0
Kinetic solubility	15.7 μM
Permeability	2.38 × 10 ⁻⁶ cm/s
t _{1/2} (human/rat/mouse)	12/9/20 min

^aCalculated with Pipeline Pilot workflow application (Accelrys) at pH 7.4.^bCalculated with ChemDraw.

Author Manuscript

Author Manuscript

Author Manuscript

Author Manuscript

Table 2.

Inhibition potency, selectivity profile, and stability in rat, mouse, and human liver microsomes of compounds derived from Scheme 1.

Compd.	R ₁	R ₂	X	IC ₅₀ (nM)*				Microsome stability (min)			
				MMP-13	MMP-2	MMP-8	clogD _{7.4} ^a	clogP ^b	rat	mouse	human
2	Me		F	2.7±0.6	>5000	>5000	4.2	3.0	9	20	12
9			H	12.9±1.1	500±100	140±25.0	2.2	2.6	61	39	>120
10			H	14.4±1.7	362±82.0	>5000	2.2	2.6	nd	nd	nd
11			H	7.1±0.6	172±23.0	83±26.0	2.97	2.6	45	>120	>120

Author Manuscript

Author Manuscript

Author Manuscript

Author Manuscript

Compd.	R ₁	R ₂	X	IC ₅₀ (nM)*					Microsome stability (min)			
				MMP-13	MMP-2	MMP-8	clogD _{7.4} ^a	clogP ^b	rat	mouse	human	
12			H	6.9±1.2	232±32.0	117±51.0	2.97	2.6	nd	nd	nd	
13			H	5.5±0.6	114±18.0	38±19.0	2.92	2.6	nd	nd	nd	
14			H	6.4±0.9	219±28.0	110±46.0	2.97	2.6	42	>120	>120	
15			H	7.3±0.8	187±38.0	35±16.0	3.5	2.8	19	65	64	

Author Manuscript

Author Manuscript

Author Manuscript

Author Manuscript

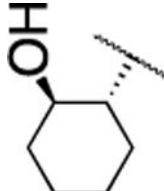
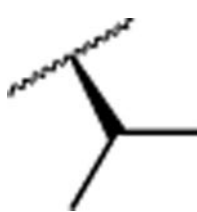
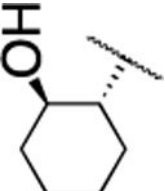

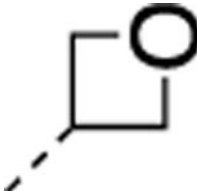

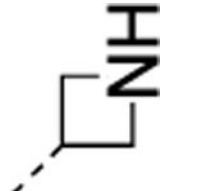

Compd.	R ₁	R ₂	X	IC ₅₀ (nM)*				Microsome stability (min)			
				MMP-13	MMP-2	MMP-8	clogD _{7.4} ^a	clogP ^b	rat	mouse	human
16			H	7.8±1.0	189±36.0	29±13.0	3.5	2.8	nd	nd	nd
17			F	9.1±0.4	> 5000	1600±470	4.7	3.6	9	38	18
18			H	1.6±0.6	> 5000	> 5000	4.9	3.9	34	26	14
19			H	> 5000	nd	nd	4.9	3.9	nd	nd	nd

Author Manuscript

Author Manuscript

Author Manuscript

Author Manuscript

Compd.	R ₁	R ₂	X	IC ₅₀ (nM)*				Microsome stability (min)			
				MMP-13	MMP-2	MMP-8	clogD _{7.4} ^a	clogP ^b	rat	mouse	human
20			F	> 5000	nd	nd	5.1	4.1	nd	nd	nd
21			F	5.1±0.3	> 5000	> 5000	5.1	4.1	42	22	13
22			F	4.4±1.0	> 5000	> 5000	3.9	3.6	29	9	27
23			F	20±1.2	>5000	>5000	2.4	3.6	25	>120	>120


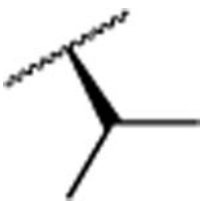
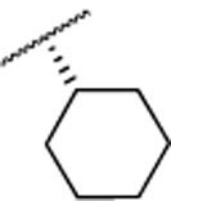
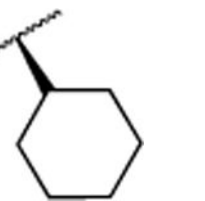
* The IC₅₀ values for MMP-1, MMP-9 and MT1-MMP for all compounds are > 5 μM. nd = not determined.

^a Calculated with Pipeline Pilot workflow application (Accelrys) at pH 7.4.

^b Calculated with ChemDraw.

Table 3.

In-vitro biological evaluation of compounds derived by Scheme 2

Compd.	R	IC ₅₀ (nM) *				Microsome stability (min)					Collagen cleavage (20 μM)
		MMP-13	MMP-2	MMP-8	clogD _{7,4} ^a	clogP ^b	rat	mouse	human		
2		2.7±0.6	>5000	>5000	4.2	3.0	9	20	12	>90%	
25		257±35.0	>5000	>5000	4.2	3.0	8	11	6	<40%	
26		4.4±1.5	>5000	>5000	5.2	4.2	4	22	7	>90%	
27		159±59.0	>5000	>5000	5.2	4.2	nd	nd	nd	>90%	

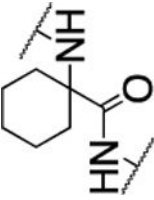
Compd.	R	IC ₅₀ (nM)*					Microsome stability (min)				
		MMP-13	MMP-2	MMP-8	clogD _{7,4} ^a	clogP ^b	rat	mouse	human	Collagen cleavage (20 μM)	
28		2.4±0.1	128±23.0	17±1.9	4.5	3.4	nd	nd	8	>90%	
29		289±24.0	nd	nd	4.5	3.4	nd	nd	nd	>90%	
30		1.9±0.3	936±190	113±23.0	3.5	1.8	4	52	29	>90%	
31		8.5±1.4	>5000	832±53.0	3.9	2.5	13	31	74	>90%	
32		2.5±0.5	584±21.0	128±47.0	3.1	1.8	15	33	59	>90%	

Author Manuscript

Author Manuscript

Author Manuscript

Author Manuscript

Compd.	R	IC ₅₀ (nM) [*]					Microsome stability (min)					Collagen cleavage (20 μM)
		MMP-13	MMP-2	MMP-8	clogD _{7,4} ^a	clogP ^b	rat	mouse	human			
33		43.2±4.8	>5000	>5000	4.8	3.7	nd	nd	nd	nd	<10%	

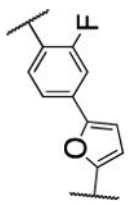
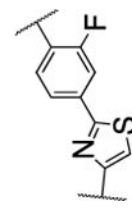
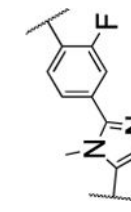
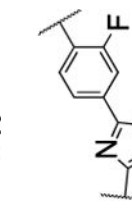
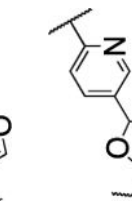
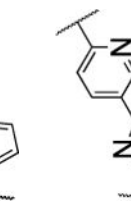
^{*}The IC₅₀ values for MMP-1, MMP-9, and MT1-MMP are >5 μM for all compounds. nd = not determined.

^aCalculated with Pipeline Pilot workflow application (Accelrys) at pH 7.4.

^bCalculated with ChemDraw.

Table 4.

In-vitro biological evaluation of compounds derived by Scheme 4.

Compd.	R ₁	IC ₅₀ (nM) *						Microsome stability (min)				Collagen cleavage (20 μM)
		MMP-13	MMP-2	MMP-8	eLogD _{7.4} ^a	eLogP ^b	rat	mouse	human			
2		2.7±0.6	>5000	>5000	4.2	3.0	9	20	12	>90%		
52		7.1±0.8	>5000	1100±236	3.6	3.3	9	26	12	>90%		
53		>5000	nd	nd	3.3	2.7	14	110	59	nd		
54		18±4.9	nd	nd	3.2	2.5	10	31	21	40%		
55		38±7.5	>5000	>5000	3.3	1.5	4	12	96	65%		
56		148±8.5	nd	nd	3.8	3.3	5	20	82	nd		

Author Manuscript

Author Manuscript

Author Manuscript

Author Manuscript

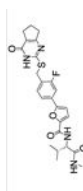
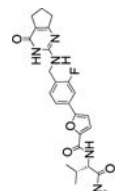
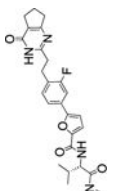
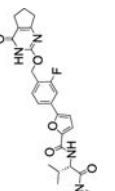
* The IC50 values for MMP-1, MMP-9, and MT1-MMP are >5 μ M for all compounds. nd = not determined.

^a Calculated with Pipeline Pilot workflow application (Accelrys) at pH 7.4.

^b Calculated with ChemDraw.

Table 5.

In-vitro biological evaluation of compounds derived from Scheme 6.

Compd.	MMP-13 IC ₅₀ (nM) [*]	Microsome stability (min)				Collagen cleavage at 20µM	
		clogD _{7.4} ^a	colgp ^b	rat	mouse		human
2 	2.7±0.6	4.2	3.0	9	20	12	>90%
72 	6.4±2.1	3.0	2.4	22	10	17	>90%
73 	18.7±2.4	3.6	2.7	7	14	26	>90%
74 	697±83.0	3.7	2.6	7	7	14	<5%

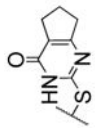
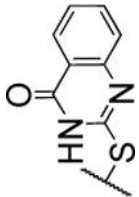
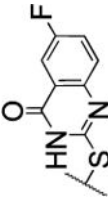
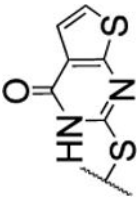
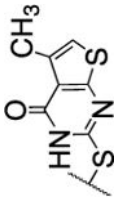
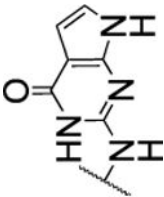
^{*} The IC₅₀ values for MMP-1, MMP-2, MMP-8, MMP-9, and MT1-MMP are >5 µM for all compounds.

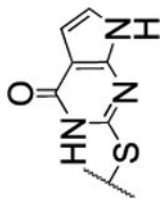
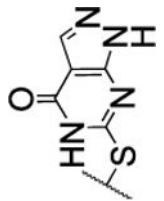
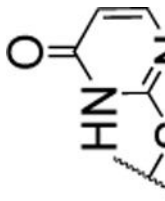
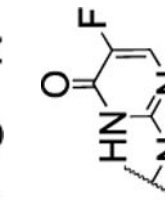
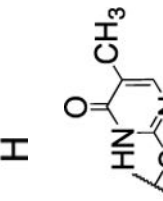
^a Calculated with Pipeline Pilot workflow application (Accelrys) at pH 7.4.

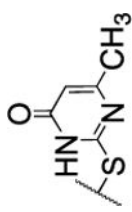
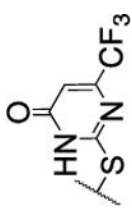
^b Calculated with ChemDraw

Table 6.

In-vitro biological evaluation of compounds derived from Scheme 8.

Compd.	R ₁	IC ₅₀ (nM) [†]				Microsome stability (min)			
		MMP-13	MMP-2	MMP-8	logD _{7,4} ^a	logP ^b	rat	mouse	human
2		2.7±0.6	>5000	>5000	4.2	3.0	9	20	12
99		9.4±1.7 [*]	>5000	400±38.0	4.6	3.6	nd	nd	nd
100		2.5±0.5 [*]	>5000	270±38.0	4.8	3.8	4	28	8
101		8.4±1.4	nd	nd	4.4	3.4	6	29	14
102		13±2.7	nd	nd	4.9	3.9	4	28	13
103		>5000	nd	nd	3.7	2.9	nd	nd	nd

Compd.	R ₁	IC ₅₀ (nM) [†]					Microsome stability (min)				
		MMP-13	MMP-2	MMP-8	logD _{7,4} ^a	logP ^b	rat	mouse	human		
104		2000±850	nd	nd	3.7	2.9	nd	nd	nd		
105		274±29.0	nd	nd	3.1	2.4	nd	nd	nd		
106		153±13.0	nd	nd	3.1	2.0	33	57	160		
107		2600±480	nd	nd	1.7	1.9	nd	nd	nd		
108		1300±110	nd	nd	3.5	2.5	nd	nd	nd		

Compd.	R ₁	IC ₅₀ (nM) [†]				Microsome stability (min)			
		MMP-13	MMP-2	MMP-8	logD _{7,4} ^a	logP ^b	rat	mouse	human
109		88±5.6	nd	nd	3.7	2.5	nd	nd	nd
110		1200±200	nd	nd	4.3	3.0	41	43	>120

^{*}IC₅₀ values for MMP-1, MMP-9, and MTI-MMP > 5 μM.

[†]Some selectivity profiles among MMP-1, MMP-2, MMP-8, MMP-9 and MTI-MMP were not determined due to either low activity or poor microsomal stability of the compound. nd = not determined.

^aCalculated with Pipeline Pilot workflow application (Accelrys) at pH 7.4.

^bCalculated with ChemDraw.

Table 7.Permeability and solubility of compounds selected by their *in vitro* microsomal stability.

Compd.	Permeability [nm/s]	Retention	Solubility [μ M]
2	23.8	47%	15.5
21	3.4	61%	nd
22	13.2	34%	nd
23	0.3	30%	58.7
28	72.9	17%	16.0
31	21.1	24%	47.5
52	34.3	40%	nd
72	1.98	45%	36.7

Author Manuscript

Author Manuscript

Author Manuscript

Author Manuscript

Table 8.Rat *in vivo* PK parameters of selected MMP-13 inhibitors.

Compd.	T _{1/2} (h)	c _{max} (μ M)	Cl (mL/min/kg)
2	2.9	47.6	0.18
28	2.6	59.4	0.25
30	2.8	75.6	0.16
31	3.0	56.8	0.23
32	2.4	56.9	0.22

Dose: IV, 1 mg/kg; formulation = 1 mg/mL in 10/10/80 DMSO/Tween 80/water.

Author Manuscript

Author Manuscript

Author Manuscript

Author Manuscript

Table 9.

CYP isoform inhibition of selected MMP-13 inhibitors.

% Inhibition of human CYPs at 10 μ M				
Compd.	1A2	2C9	2D6	3A4
2	8	60	-33	16
28	-2	75	-35	43
30	-5	35	-31	-6
31	-12	29	-45	-17
32	-3	25	-19	-3

Author Manuscript

Author Manuscript

Author Manuscript

Author Manuscript

Table 10.

Comparison of PK properties of compounds **2** and **31**.

Property	Compound 2	Compound 31
Kinetic solubility	15.7 μ M	47.5 μ M
Permeability / Retention	23.8 nm/s / 47%	21.1 nm/s / 24%
$t_{1/2}$ (human/rat/mouse)	12/9/20 min	74/13/31 min
CYP 3A4 inhibition at 10 μ M	16%	No inhibition